Industrial Engineering Journal
ISSN: 0970-2555
Volume : 53, Issue 6, No.1, June : 2024

MMWAVE BEAMFORMING IN MASSIVE MIMO SYSTEMS WITH MACHINE LEARNING TECHNIQUES

Mr.A.Sammaiah, Research Scholar, Department of Electronics and Communication Engineering,Chaitanya Deemed to be University,Hanamkonda.
Dr M. Pranay Kumar, Associate Professor, Department of Electronics and Communication Engineering, Chaitanya Deemed to be University,Hanamkonda.

ABSTRACT
Next generation communication technology is 6G. Machine learning algorithms have seen extensive use recently in several industries, including health, transportation, and autonomous vehicles. The 6G issues will make use advantage of the predictive algorithms. Regarding the use of deep learning (DL) techniques in mmwave networks to secure beamforming prediction, there is no general agreement. In order to handle beamforming prediction as a multi-output regression issue, this research examines security flaws in DL for beamforming prediction utilising DNNs (deep neural networks) in 6G wireless networks. This study suggests a brand-new method for beamforming in 6G networks that makes use of massive MIMO in mmwave and a machine learning model. Here, a massive multi-user half-duplex spatiotemporal convolutional neural network (MMU_STCNN) as the network's basis for energy optimisation. The proposed technique attained MSE of 62%, BER of 51%, and spectral efficiency of 85%. Based on amount of independent data streams per user, the performance results propose using a certain mMIMO antenna design, and it is strongly advised to employ more data streams per user to meet the requirements of 6G wireless networks
Keywords: 6G network, beamforming, massive MIMO, mmwave, machine learning model.

1.Introduction:
There are not enough spectral resources to meet the need for greater data rates, which is always rising. As a result, one of the critical possibilities for beyond fifth-generation (B5G) and sixth-generation (B6G) mobile communication networks is millimeter-wave (mmWave), which has a broad spectrum between 30 GHz and 300 GHz. This has recently aroused and received massive research attention [1]. Although mmWave transmissions suffer from high path loss (PL), shorter wavelengths allow large-scale antennas to be packed into a compact mmWave device. MIMO (Massive multiple-input multiple-output) methods are utilised in mmWave communications to provide a sufficiently high SNR (signal-to-noise ratio), allowing the PL to be compensated [2]. The full-digital strategy is difficult to implement in practise due to need for one specific RF (radio frequency) chain per antenna, prohibitive hardware costs, and significant energy consumption with large antenna arrays. Although full-analog beamforming is a more energy-efficient option to full-digital beamforming in low-cost phase shifters (PSs), spectrum efficiency is often constrained by the fact that only one data stream is maintained by a single shared RF chain [3].As a result, hybrid analog/digital beamforming with a limited number of RF chains coupled to a large number of antennas has been employed in mmWave massive MIMO systems to provide beam gain and interference management while decreasing energy consumption, wire complexity, and hardware cost. Because mmWave signals are prone to interference, they are usually employed in line-of-sight (LoS) situations [4]. Links may be hindered by the obstructions on the ground as a result of the formation of LoS. Even when beamforming is used, it causes significantly reduced signal strengths at the receiving node.
As a result of the D2D networks like IoT, IIoT, and IoS' fast expansion, 5G wireless technology may soon be insufficient. The 6G wireless network, which is the next generation, will support communication requirements in the year 2030. As a result, 6G wireless technology, which allows data speeds of Terabits/sec and utilises terahertz (0.1–10 THz) wavelengths of the electromagnetic spectrum, is crucial. For optimum capacity, radio network design of 6G cellular systems should

include carrier aggregation, ultra-mMIMO, cognitive radio, THz bands, and femto cell-based heterogeneous networks [5]. Using a data-driven method and machine learning (ML) technique, these intricate structures of 5G and future technologies may be recorded. Without human involvement, the network structure can train and adjust itself to serve the various needs of the systems thanks to the powerful learning, reasoning, and intelligent recognition characteristics of ML. Security issues might arise from the integration of the ML for the 6G beyond technologies. Due to their design, wireless communication networks in particular contain security flaws. The current 5G solutions would be transferred to the AI field, more especially the ML field. For AI-based methods in 6G wireless networks, it is necessary to create safe ML solutions. Current 5G security issues, ML security vulnerabilities represent a new attack surface. Before implementing their ML models in real-world settings, researchers and corporations should fix their security issues. For the new categories of security risks in next-generation wireless communication methods, they must recognise, record, and analyse the risk [6].

II.Literarure

The employment of cutting-edge communications and AI technology is the most crucial factor for this new generation [7]. Numerous research on next-generation wireless networks as well as integration of newly developed AI tools into these networks can be found in the literature [8]. In high SNR situations, an exhaustive search technique through all beam pairs in codebooks produces ideal beam pairs, but it comes with unacceptable high latency and overhead. However, there is no assurance that the cell edges will be covered by hierarchical search methods, despite their lower overhead. To address these issues, context information (CI)-based beam alignment techniques that take advantage of contextual data such user location have been developed[9]. One method based on Bayesian decision theory put out in [10] to lessen the consequences of incomplete position information at both ends. The authors of [11] offer a beam selection technique that also calculates the receiver's position and orientation at each stage of the beam alignment process, demonstrating the synergy between the position/orientation estimation and beam alignment processes. Consider channel estimate for wideband mm-Wave large MIMO methods, one of the earlier research [12]. In [13], which designs OFDM-based frequency-selective structures, the hybrid beamforming architecture was examined. [14] particularly proposes a GS-HB under hypothesis of perfect CSI. GS-HB selects precoders from a constrained codebook based on immediate channel data. For the hybrid precoder design, [15] offered a phase extraction strategy based on the same CSI assumption.

According to [16], a wideband channel's second-order spatial channel covariance matrix is used to create a unified analogue beamformer. In order to optimise several metrics, including MS assignments and transmission powers, the idea of FL (federated learning) in m-MIMO systems is presented in [17].To achieve this, decentralised, discrete-time resource optimisation using ML is carried out. [18] examines an SL technique for user placement that outperforms existing ML frameworks like the k-NN methodas well as support vector machines (SVMs). [19] presents a DL strategy to streamline the estimation of beamforming weights. Findings that have been provided show that the suggested technique may greatly lessen the complexity of weight estimation as a whole. For EE maximisation, hybrid beamforming is utilised in [20]. In same context, a low-complexity strategy based on ACE (adaptive cross-entropy)-based optimisation with low-bit phase shifters was used to solve sum rate maximisation issue. In [21], authors offer a method for implementing adaptive time-domain wideband beamforming without delay structures in the case of insufficient snapshots, which is based on the WBPNet CNN structure. To increase spectral efficiency, [22] proposes a DL-NN for hybrid precoders as well as combiners. The proposed method has the significant advantage of requiring no prior knowledge, such as channel and angle parameters. The authors of [23] use a k-NN SL technique to calculate the performance of an adaptive beamforming method in 5G multi cellular mmWave orientations, choosing the best beamforming configuration based on the desired SE in an active sector. According to statistics, this strategy

produces SE as well as EE levels equivalent to normal non-ML method, but at expense of enhanced BP.

III. System Model:

Huge MIMO THz network deployment model is depicted in Fig. 1. Downlink, where a single cell access point (AP) is connected to several users, will be primary focus in indoor office applications. Small scale as well as large scale fading channel methods, antenna array layout, power delay profile analysis are all presented.

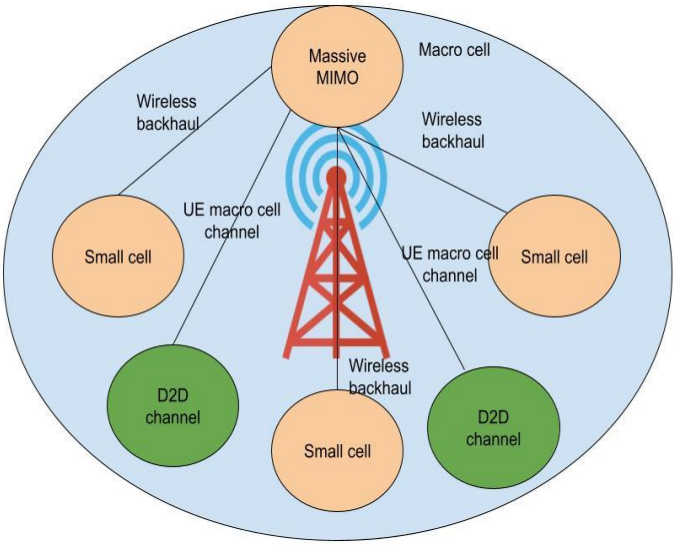

Figure-1 Proposed 6G Beamforming model

We investigate a cell-free mmWave massive MIMO network in which M randomly distributed APs are activated to serve K single-antenna MSs, each outfitted with an array of N antennas as well as linked to a CPU. Each frame has three phases: UL training, UL payload data transmission, DL payload data transmission. All MSs send training pilots during UL training phase, allowing active APs to determine propagation channels to each MS in network channel estimations are then utilised to construct precoding filters that direct DL payload data transmission as well as to identify signals broadcast from MSs during UL payload data transmission phase.

We investigate a single-user UM-MIMO network in which both BS as well as user employ ULA with multiple antennas. The transmitter, we assume, has Nt antennas, while receiver, we assume, has Nr antennae. This is also known as a multi-stream point-to-point network with Ns data streams. Because of limited number of transmit/receive RF chains, completely digital beamforming. Instead, we study a two-stage hybrid digital as well as analogue beamforming design at BS as well as user terminal. The signal that is now being transmitted is as follows by equation (1)

$$\mathbf{x} = \mathbf{F}_{RF}\mathbf{F}_{BB}\mathbf{S}$$
$$E[\mathbf{s}\mathbf{s}^H] = \left(\frac{1}{N_s}\right)\mathbf{I}_{N_s} \quad (1)$$

Received signal r given after decoding as by equationn (2)

$$\mathbf{r} = \sqrt{\rho}\mathbf{W}_{RF}^{H}\mathbf{W}_{BB}^{H}\mathbf{H}\mathbf{x} + \mathbf{W}_{RF}^{H}\mathbf{W}_{BB}^{H}\mathbf{n} \quad \mathbf{(2)}$$

***III a. Channel model*:** This study's channel method is based on S-V method with a THz-band modification. Furthermore, based on availability of CSI, HBF architectures can be classified into two variants: HBF with full-instantaneous CSI as well as HBF with averaged CSI.

In this study, we just look at the first case and leave the second for further research. In practise, CSI may be precisely and efficiently obtained at the receiver via channel estimation as well as then shared with transmitter utilizing significant feedback mechanisms by equation (3)

Industrial Engineering Journal
ISSN: 0970-2555
Volume : 53, Issue 6, No.1, June : 2024

$$\mathbf{H} = \sqrt{\frac{N_t N_r}{N_{cl} N_{ray}}} \sum_{i=1}^{N_{cl}} \sum_{l=1}^{N_{ray}} \alpha_{ij} \mathbf{a}_r(\phi_{il}^r, \theta_{il}^r) \mathbf{a}_i(\phi_{il}^t, \theta_{il}^t)^H \quad (3)$$

As a result, the array response vector for the i[th] cluster's l[th] ray can be written as equation (4)

$$\mathbf{a}(\phi_{il}, \theta_{il}) = \frac{1}{\sqrt{N}} \left[1, \dots, e^{j\frac{2\pi}{\lambda} d(p \sin \phi_{il} \sin \theta_{ll} + q \cos \theta_{il})}, \dots, e^{j\frac{2\pi}{\lambda} d((\sqrt{N}-1) \sin \phi_U \sin \theta_\mu + (\sqrt{N}-1) \cos \theta_{ll})}\right]^T \quad (4)$$

III b. MMU_STCNN:

According to transmission method, received signals in first as well as second sub-blocks of b[th] block is expressed as equation (5)

$$\mathbf{y}^{(1)}(b,n) = \sum_{k=1}^{K} \mathbf{H}_k^{(1)}(b,n) \mathbf{x}_k^{(1)}(b,n) + \mathbf{z}^{(1)}(b,n), n \in [0, KN_M - 1]$$

$$\mathbf{y}^{(2)}(b,n) = \sum_{k=1}^{K} \mathbf{H}_k^{(2)}(b,n) \mathbf{x}_k^{(2)}(b,n) + \mathbf{z}^{(2)}(b,n), n \in [0, L-1] \quad (5)$$

In these two equations, channel coefficients matrices between BS as well as k[th] user are thought to be independent. Active antenna indices in first sub-block are used since they follow a preset pattern. As a result a straight forward discrepancy detection method for first sub-block. And Second sub-block is found. In contrast to first, it sends information utilising both M-PSK symbols as well as active antenna indices.

Purpose of this study is to estimate the active antenna indices and transmitted M-PSK symbols for all users. For the second sub-block, we will suggest a two-step differential MRC detection approach in following paragraphs. It is demonstrated that suggested detector outperforms its coherent counterpart. To reconstruct channel coefficients for remaining UTs in the first stage that did not contribute to CE, suggest CNN-based stage.Number of resolvable paths is generally in range of 3 5 due to limited scattering qualities of the mmWave propagation environment. Furthermore, propagation gain for line-of-sight path is significantly greater than propagation gains for other Non-LOS paths. The channel coefficients are obtained by evaluating AoAs, AoDs, and propagation paths. As a result, (1) and (4) are just the LOS paths between BS as well as RIS, LOS paths between the RIS and the UTs. (1) and (4) are mutually exclusive by equation (6)

$$\mathbf{H}_{r,c} = \alpha_{B,R}^{(0)} \mathbf{a}_{B,R}\left(\phi_{B,R}^{(0)}\right) \mathbf{a}_{B,R}^H\left(\theta_{B,R}^{(0)}\right) \mathbf{\Omega} \alpha_{R,M}^{(0)} \mathbf{a}_{R,M}\left(\theta_{R,M}^{(0)}\right) = \alpha^{(0)} \mathbf{a}_{B,R}\left(\phi_{B,R}^{(0)}\right) \quad (6)$$

where $\alpha^{(0)} = \alpha_{B,R}^{(0)} \alpha_{R,M}^{(0)} \mathbf{a}_{B,R}^H\left(\theta_{B,R}^{(0)}\right) \mathbf{\Omega} \mathbf{a}_{R,M}\left(\theta_{R,M}^{(0)}\right)$ is effective propagation path gain

Residual output is utilised to uncover relationships between diverse auxiliary data instead of straightforward output. A natural image is equivalent to the composite channel matrix. Furthermore, the first stage's incomplete CSI can be regarded as an image with missing portions.

As a result, we can minimize either N or K throughout sounding period by adding a binary mask to picture instead of channel matrix. Figure 2 depicts second stage of proposed technique. Dilated convolutions are used in the DL-based technique to improve contextual data by keeping size of convolution kernel filter constant while extending size of receptive field.

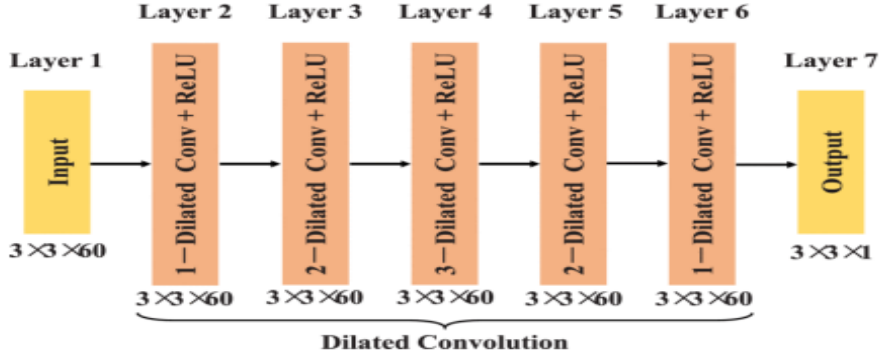

Figure-2 proposed CNN model

Industrial Engineering Journal
ISSN: 0970-2555
Volume : 53, Issue 6, No.1, June : 2024

The drop out layers have been deleted for visual clarity. As input, N is given 2 vectors of size ($N_{t,1}$).1 Inputs are normalised resolved components of the F_{opt} columns. Two independent input layers receive the phase and magnitude inputs individually. In each branch, three 1D convolution blocks follow input layer, each containing 2 convolution layers followed by a max-pooling layer.

To prevent undesirable noise from being incorporated in the early convolution layers, the initial convolution block does not have zero padding. The remaining convolution blocks have no padding to avoid having extremely small feature dimensions. Hundreds of model training sessions revealed that utilising fewer than three blocks lowers DNN accuracy. Using four or more blocks, on the other hand, causes extra computing cost as well as gradient underflow with no discernible improvement in accuracy.

To establish the exact number of separable convolution layers employed in method, we conduct extensive trials and errors. Following convolution feature extraction, we flatten branches as well as construct a dense layer. The two branches are then joined and passed through two more thick layers. A bidirectional LSTM block with two LTSM layers is then used. We observed that only two LSTM layers are required to attain the best accuracy after hundreds of training simulations.

First, the unidirectional RNN updates the hidden layers based on data from input layer and activation state. Unidirectional RNN, on the other hand, can only learn from the past. In this paper, a bidirectional method is employed to enhance RNN. In this merging, one side learns prior state, while other learns future state. Two outputs are then combined to get a more accurate approximation. Because of its bidirectional capabilities, the LSTM may train each input sequence in independent forward as well as backward states.

When compared to the traditional LSTM technique, this improves LSTM's capacity to extract more contextual beam index information. For backward as well as forward states, each of the bidirectional units takes a similar strategy. Another constraint for RNN networks is gradient vanishing issue for long data sequences during training. As a result, LSTM networks are employed to overcome this issue by incorporating memory blocks composed of multiplicative gates and self-connected memory cells, allowing for learning of long-term dependencies. First, consider input state of LSTM cell as well as outer processing stage located between layers.

Input data is first processed by bidirectional forward as well as backward layers for outer stage between the layers in order to find the hidden states. These values offer the context for beam indices as well as power levels. In this case, bidirectional feature allows LSTM to receive further beam index contextual data by accessing the present as well as future time steps by transitioning between backward as well as forward states, as opposed to standard LSTM. Consider data in LSTM cell. Cell state c_t at time t, which decides data conveyed to next sequence, is initially adjusted by g^f_t in sigmoid layer placed beneath it, which is subsequently altered by g mod t, which supplies new candidate cell state, for inner stage of LSTM unit. At time step t, equations (7) express the c_t, g^f_t, g^{in}_t, g^{mod}_t , and g^{out}_t formulations, respectively by equation (7)

$$
\begin{aligned}
c_t &= g_t^f c_{t1} + g_t^{\text{in}}\, g_t^{\text{mod}} \\
g_t^f &= \sigma_g\left(W_f[\eta_{t-1}, x_t] + \beta_f\right) \\
g_t^{\text{in}} &= \sigma_g\left(W_{\text{in}}[\eta_{t-1}, x_t] + \beta_{\text{in}}\right) \\
g_t^{\text{mod}} &= \tanh\left(W_c[\eta_{t-1}, x_t] + \beta_c\right) \\
g_t^{\text{out}} &= \sigma_g\left(W_{\text{out}}[\eta_{t-1}, x_t] + \beta_{\text{out}}\right)
\end{aligned}
\tag{7}
$$

As a result, g mod t is activated with a tanh activation function with a range of [1, 1], allowing cell state to forget memory. Model's total training parameters are made up of four layers and one thick layer. The dropout layer controls weight of hidden layers, with a dropout regularisation rate of 0.2 applied to each regularize layer. 350 epoche are utilised to train the model over the course of two weeks. Because LSTM cells have long-term memory, a data structure is built with 60 time steps of

10 minutes each, single output is produced. As a result, each training stage contains 60 components from the previous training set for every sample obtained.
First 60 samples are required to accurately identify the next best beam index during testing. The overall purpose of training is to generate weight matrices as well as bias vectors that minimise loss function at each training time step. Equation 7 is outcome of applying reward shaping rule to Q-learning update method.Equation 7 will allow us to enhanced learning by delivering new knowledge about problem to Q-learning agent. This extra information could originate from anywhere, including human problem-solving expertise, heuristic functions, or information retrieved by the agent by Equation (8)

$$Q(s_t, a_t) \leftarrow Q(s_t, a_t) + \alpha \left[R_{t+1} + F + \gamma \max_a Q(s_{t+1}, a) - Q(s_t, a_t)\right] \quad (8)$$

Because of the use of this potential function, optimal policy in MDP(M 0 = (S, A, T, γ, R+ F)) remains optimal in old MDP(M = (S, A, T, γ, R)). γ remained unaltered in equation 3 and all of its extended equations as well as same value as it did in old MDP. Other studies in literature build on this putative role as well by equation (9)

$$\eta(\pi) = \mathbb{E}_{s_0, a_0, \ldots}\left[\sum_{t=0}^{\infty} \gamma^t r(s_t)\right], \text{ where}$$

$$s_0 \sim \rho_0(s_0), a_t \sim \pi(a_t \mid s_t), s_{t+1} \sim P(s_{t+1} \mid s_t, a_t) \quad (9)$$

The usual description state action value function Q_π, V_π value function, advantage function A_π will be used by equation (10)

$$Q_\pi(s_t, a_t) = \mathbb{E}_{s_{t+1}, a_{t+1}, \ldots}\left[\sum_{l=0}^{\infty} \gamma^l r(s_{t+l})\right]$$

$$V_\pi(s_t) = \mathbb{E}_{a_{t,s}, +1, \ldots}\left[\sum_{l=0}^{\infty} \gamma^l r(s_{t+l})\right]$$

$$A_\pi(s, a) = Q_\pi(s, a) - V_\pi(s), \text{ where}$$

$$a_t \sim \pi(a_t \mid s_t), s_{t+1} \sim P(s_{t+1} \mid s_t, a_t) \text{ for } t \geq 0 \quad (10)$$

The following helpful identity describes another policy's expected return in terms of advantage over, collected over time steps by equation (11)

$$\eta(\tilde{\pi}) = \eta(\pi) + \mathbb{E}_{s_0, a_0, \ldots \sim \tilde{\pi}}[\textstyle\sum_{t=0}^{\infty} \gamma^t A_\pi(s_t, a_t)]_1 \quad (11)$$

where notation $\mathbb{E}_{s_0, a_0, \ldots \sim \tilde{\pi}}[\ldots]$actions are sampled at $a_t \sim \tilde{\pi}(\cdot \mid s_t)$. Let $\rho_\pi$be discounted visitation frequencies by equation (12)

$$\rho_\pi(s) = P(s_0 = s) + \gamma P(s_1 = s) + \gamma^2 P(s_2 = s) + \cdots \quad (12)$$

The fundamental goal of our NN-based method is to obtain a high sum rate while minimising delay. In this instance, latency refers to time it takes neural network to estimate beamforming matrices. Because the transmitter and receiver send as well as receive data using hybrid beamforming, delay is proportional to time necessary to produce beamforming matrices.

III c. ***Experimental analysis:***

We consider the case when M = 50 APs and K = 30 MSs are distributed uniformly and randomly throughout an 11 km2 area. The experimental results are reviewed, specifications utilized for analysis are BER, MSE, spectral efficiency in terms of interference alignment, MSE, BER, spectral efficiency,poer consumption. The comparative carried out based on number of cells as well as number of users. We pay attention to the fact that channel features like PDP may be seen as a fingerprint for UE location in a cell-specific way with certain surroundings. In other words, PDP can describe a UE's location with a certain g^N_B and environment. Furthermore, because mmWave cells support tiny regions with high throughput whereas sub-6 GHz cells support large areas, it is

reasonable to consider that UE attempting to found a mmWave link is connected to sub-6 GHz networks.
Cumulative distribution function (CDF) curves of SE, EE, BP, and the topology's maximum number of REs are shown. Table 1 summarises all simulation parameters. Non-uniform traffic is predicted because goal of adaptable beamforming system is to provide QoS to MSs in cases of enhanced spatial appropriation. In this case, there is one trouble area zone for each BS, and its location may change depending on the MC preview.
The problem area region sweep is equal to 0.1R, where R is span of every BS in direction. Two beamforming approaches have been considered in each of the presented results: The previously depicted calculation selects the appropriate BC per case in main case. Previous segment's ML structure is used in the following scenario, referred to as ML for remainder of paper. Furthermore, two traffic conditions are expected: In general, all PRBs per MS use the QPSK adjustment type.
Table 1. Simulation parameters

Parameter	**Value/Assumption**
Tiers of cells	2
Subcarrier spacing (kHz)	60
Total bandwidth (MHz)	100
Antenna elements per MS	2
Pathloss method	UMa
Cell radius (m)	500
Carrier frequency (GHz)	28
Traffic scenario-1	QPSK modulation per MS's PRB
Beamforming configuration	51
Traffic scenario-2	Per PRB, 50% of MSs have QPSK. Per PRB
Mc snap shorts	10^4

Table-2 Comparative based on various network cases

Cases	**Techniques**	**MSE**	**BER**	**Power consumption**	**Spectral efficiency**
Number of cells	CNN	55	45	58	77
	ELM	58	48	60	79
	MMU_STCNN	61	49	65	82

Table-2 analysis based on number of cells and number of users. Parameters has been analysed are MSE, BER, spectral efficiency and power consumption. Existing technique compared are CNN and ELM.

Industrial Engineering Journal
ISSN: 0970-2555
Volume : 53, Issue 6, No.1, June : 2024

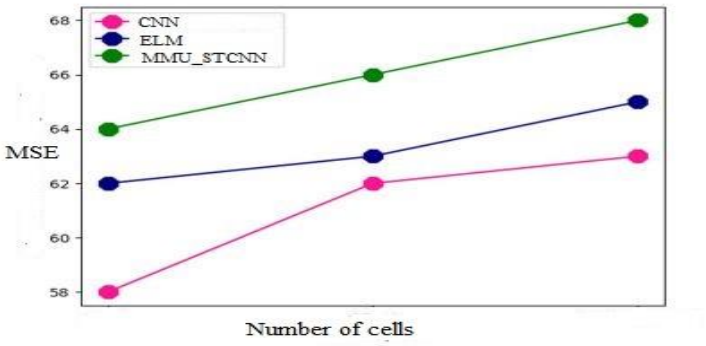

Figure-3 Comparison of Number of cells *vs* MSE

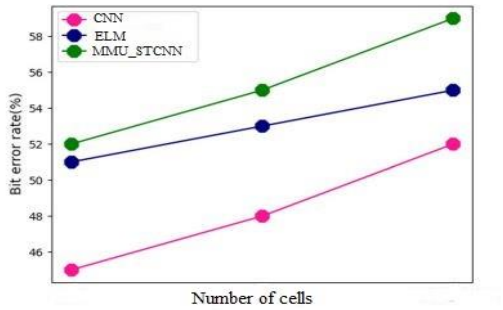

Figure-4 Comparison of Number of cells *vs* BER

Figure 3 and Figure 4 shows comparative for number of cells. Proposed technique attained MSE of 61%, BER of 49%, existing CNN attained MSE of 55%, BER of 45%, ELM attained MSE of 58%, BER of 48%. the likelihood that k-th most likely beam index is best beam index in building as well as schoolyard. It is worth noting that it is PMF of B_k selection correctness.

When sub-6 GHz transmission capacity are 20, 40, and 50 MHz, optimal bar is determined by a single shot with probabilities of 0.72, 0.76, and 0.79. In the schoolyard, the correctnesses of a single shot shaft determination are 0.60, 0.63 and 0.66, with sub-6 GHz transfer speeds of 20, 40, and 50 MHz. Two patterns emerge from this result. First and foremost, the proposed technique performs better with the increased transfer speed of sub-6 GHz channel. Explanation is that testing speeds for 40 and 50 MHz frameworks are faster than for 20 MHz frameworks. This indicates that PDP, p is obtained with a higher aim as well as DNN can contain more information. B_k-determination can overcome the problem of limited sub-6 GHz data transport capability. Choosing the bar from three applicants, for example, yields exactnesses of 0.92, 0.93, and 0.95 in structural region with sub-6 GHz transmission capabilities of 20, 40, and 50 MHz.

Industrial Engineering Journal
ISSN: 0970-2555
Volume : 53, Issue 6, No.1, June : 2024

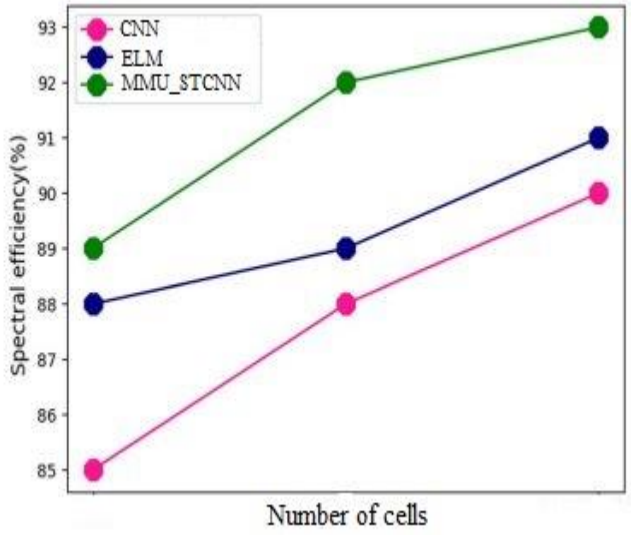

Figure-5 Comparison of Number of cells *vs* Spectral efficiency

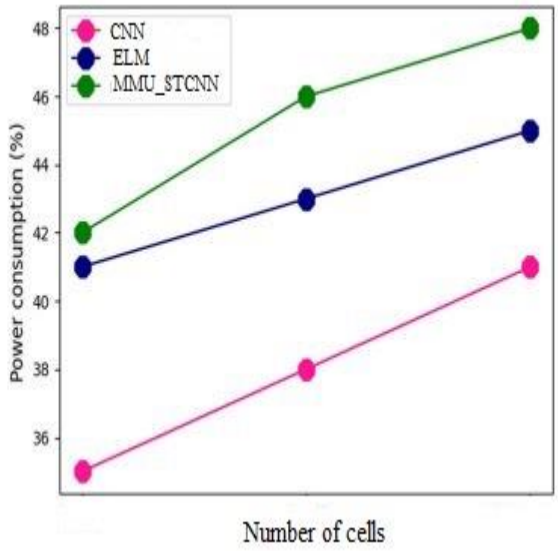

Figure-6 Comparison of Number of cells vs Power consumption

From above Figure 5 and Figure 6 comparative are carried out based on number of users. Proposed technique spectral efficiency of 82% and power consumption of 65% , existing CNN attained spectral efficiency of 77% and power consumption of 60%, ELM attained and spectral efficiency of 75% and power consumption of 57%.

Essentially, there is a trade off on choice of container measures, whose ideal setting relies upon dataset size. From one viewpoint, bigger receptacle sizes permit more information tests per container, which brings about getting better measurements for development of the rundown of shaft applicants. Then again, however, bigger receptacles bring about lower spatial goal as well as packaging together of positions for which ideal bar matches are essentially unique. Presentation of 64-point range-point arrangement needs 10 − 20% of information for beginning to soak, while different arrangements need around 20 − 30% of preparation information. This may be because of more straightforward interpretability of high resolution range-point maps for pillar expectation task, possibly requiring less learning and change. Radar-shape begin to soak especially late, and may marginally increment with additional information, sign a possible advantage from a bigger dataset or more perplexing models.

IV.*Conclusion*:

This research propose novel technique in beamforming analysis for 6G network with energy optimization using massive multi-user half-duplex spatio temporal convolutional neural network (MMU_STCNN).The results show that as compared to conventional non-ML framework, ML adaptive beamforming may greatly enhance SE. BP as well as radiating elements (REs) for high data rate services are enhanced as a result of this enhancement, but the related increase ratios are substantially lower than the SE (spectral efficiency) improvement ratio. In example, the SE may achieve up to 5.3 Mbps/W with 21.6 Mbps per active user as well as ML adaptive beamforming, which is a substantial improvement over non-ML scenario.While ML aided beamforming can greatly speed up overall execution times, beamforming is carried out in accordance with a preset set of configurations are increase spatial coverage for a range of traffic distributions. Numerous simulations at the system level were run, and the findings include a range of requests for throughput requirement per active user. The proposed technique attained MSE of 62%, BER of 51%, and spectral efficiency of 85%.

V.References:

1. Deepanram kumar, P., & Jaisankar, N. (2022). BlockCRN-IoCV: Secure Spectrum Access and Beamforming for Defense Against Attacks in mmWave Massive MIMO CRN in 6G Internet of Connected Vehicles. *IEEE Access*, *10*, 74220-74243.
2. Pari, D., & Natarajan, J. (2022). Secure Spectrum Access, Routing, and Hybrid Beamforming in an Edge-Enabled mmWave Massive MIMO CRN-Based Internet of Connected Vehicle (IoCV) Environments. *Sensors*, *22*(15), 5647.
3. Du, J., Zhang, Y., Chen, Y., Li, X., Cheng, Y., & Rajesh, M. V. (2021). Hybrid beamforming NOMA for mmWave half-duplex UAV relay-assisted B5G/6G IoT networks. *Computer Communications*, *180*, 232-242.
4. Murshed, R. U., Ashraf, Z. B., Hridhon, A. H., Munasinghe, K., Jamalipour, A., & Hossain, M. F. (2023). A CNN-LSTM-based Fusion Separation Deep Neural Network for 6G Ultra-Massive MIMO Hybrid Beamforming. *IEEE Access*.
5. Lavdas, S., Gkonis, P. K., Tsaknaki, E., Sarakis, L., Trakadas, P., & Papadopoulos, K. (2023). A Deep Learning Framework for Adaptive Beamforming in Massive MIMO Millimeter Wave 5G Multicellular Networks. *Electronics*, *12*(17), 3555.
6. Tajallifar, M., Sharafat, A. R., &Yanikomeroglu, H. (2023). Robust and Feasible QoS-Aware mmWave Massive MIMO Hybrid Beamforming. *IEEE Transactions on Wireless Communications*.
7. Kuzlu, M., Catak, F. O., Cali, U., Catak, E., & Guler, O. (2023). Adversarial security mitigations of mmWave beamforming prediction models using defensive distillation and adversarial retraining. *International Journal of Information Security*, *22*(2), 319-332.
8. Zhang, Y., Liu, A., Li, P., & Jiang, S. (2022). Deep learning (DL)-based channel prediction and hybrid beamforming for LEO satellite massive MIMO system. *IEEE Internet of Things Journal*, *9*(23), 23705-23715.
9. Vaigandla, K. K., Rani, B. S., Srikanth, K., Mounika, T., & Karne, R. (2021). Millimeter wave communications: Propagation characteristics, beamforming, architecture, standardization, challenges and applications. *Design Engineering*, *9*, 10144-10169.
10. Pang, L., Li, Y., Zhang, Y., Shang, M., Chen, Y., & Wang, A. (2022). MGGAN-Based Hybrid Beamforming Design for Massive MIMO Systems Against Rank-Deficient Channels. *IEEE Communications Letters*, *26*(11), 2804-2808.
11. Fozi, M., Sharafat, A. R., & Bennis, M. (2021). Fast mimo beamforming via deep reinforcement learning for high mobility mmwave connectivity. *IEEE Journal on Selected Areas in Communications*, *40*(1), 127-142.

12. Lavdas, S., Gkonis, P. K., Zinonos, Z., Trakadas, P., Sarakis, L., & Papadopoulos, K. (2022). A machine learning adaptive beamforming framework for 5G millimeter wave massive MIMO multicellular networks. *IEEE Access*, *10*, 91597-91609.
13. Al Avidh, A., Sambo, Y., Ansari, S., & Imran, M. A. (2021, June). Hybrid beamforming with fixed phase shifters for uplink cell-free millimetre-wave massive MIMO systems. In *2021 Joint European Conference on Networks and Communications & 6G Summit (EuCNC/6G Summit)* (pp. 19-24). IEEE.
14. Hu, Z., Chen, Y., & Han, C. (2023). PRINCE: A Pruned AMP Integrated Deep CNN Method for Efficient Channel Estimation of Millimeter-wave and Terahertz Ultra-Massive MIMO Systems. *IEEE Transactions on Wireless Communications*.
15. Dilli, R. (2022). Hybrid beamforming in 5G nr networks using multi user massive MIMO at FR2 frequency bands. *Wireless Personal Communications*, *127*(4), 3677-3709.
16. Ma, X., Zhang, D., Xiao, M., Huang, C., & Chen, Z. (2023). Cooperative beamforming for RIS-aided cell-free massive MIMO networks. *IEEE Transactions on Wireless Communications*.
17. Xu, K., Hou, J., & Ding, Y. (2023). Hybrid Massive-MIMO and Its Practical Beamforming Implementation. *6G Wireless: The Communication Paradigm Beyond 2030*, 259.
18. Femenias, G., & Riera-Palou, F. (2021). Wideband cell-free mmWave massive MIMO-OFDM: Beam squint-aware channel covariance-based hybrid beamforming. *IEEE Transactions on Wireless Communications*, *21*(7), 4695-4710.
19. Ning, B., Tian, Z., Mei, W., Chen, Z., Han, C., Li, S., ... & Zhang, R. (2023). Beamforming technologies for ultra-massive MIMO in terahertz communications. *IEEE Open Journal of the Communications Society*, *4*, 614-658.
20. Pérez Santacruz, J., Meyer, E., Budé, R. X., Stan, C., Jurado-Navas, A., Johannsen, U., ... & Rommel, S. (2023). Outdoor mm-wave 5G/6G transmission with adaptive analog beamforming and IFoF fronthaul. *Scientific Reports*, *13*(1), 13945.
21. Elbir, A. M., Mishra, K. V., &Chatzinotas, S. (2021). Terahertz-band joint ultra-massive MIMO radar-communications: Model-based and model-free hybrid beamforming. *IEEE Journal of Selected Topics in Signal Processing*, *15*(6), 1468-1483.
22. Morsali, A., Haghighat, A., & Champagne, B. (2022). Deep Learning-Based Hybrid Analog-Digital Signal Processing in mmWave Massive-MIMO Systems. *IEEE Access*, *10*, 72348-72362.